Article

Current Biology

AstA Signaling Functions as an Evolutionary Conserved Mechanism Timing Juvenile to Adult Transition

Graphical Abstract

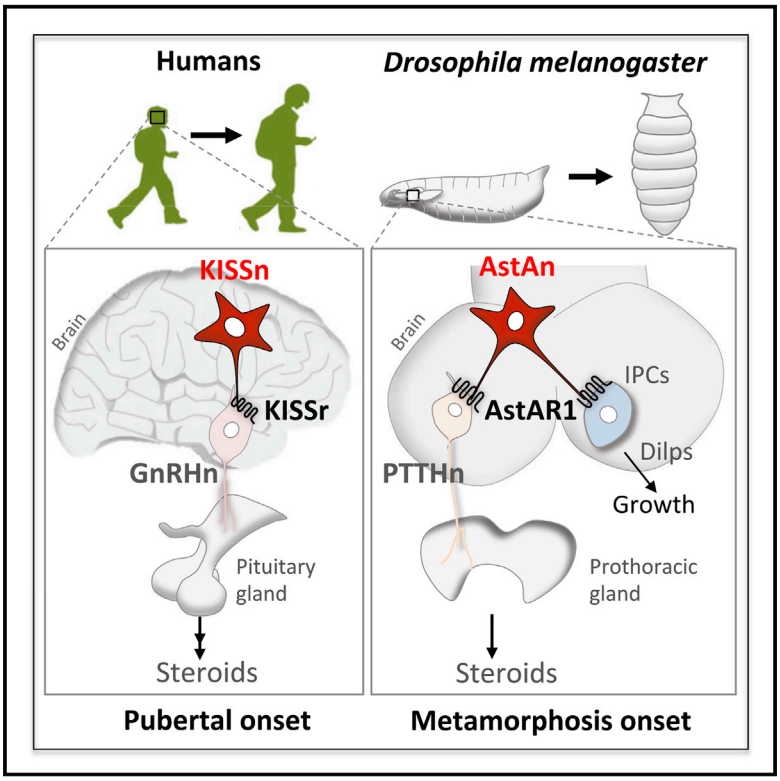

Highlights

- AstA/AstAR1 signaling times the onset of maturation by promoting PTTH secretion
- AstA/AstAR1 promotes juvenile growth by controlling Dilps secretion in the IPCs
- AstA N1 neurons coordinate growth and maturation during larval development
- AstA/AstAR1 achieves maximal activity in PTTH neurons at maturation onset

Authors

Derya Deveci, Francisco A. Martin, Pierre Leopold, Nuria M. Romero

Correspondence

pierre.leopold@curie.fr (P.L.), nromero@univ-cotedazur.fr (N.M.R.)

In Brief

In an RNAi-based screen performed in the PTTH neurons, Deveci et al. identify *Drosophila* AstA/AstAR1 as a brain signal that induces growth and the onset of maturation. AstA/AstAR1 is homologous to the ligand-receptor KISS/GPR54 that is required for human puberty, suggesting an evolutionary conserved neural circuitry controlling maturation.

Deveci et al., 2019, Current Biology *29*, 813–822
March 4, 2019
https://doi.org/10.1016/j.cub.2019.01.053

CellPress

Current Biology
Article

AstA Signaling Functions as an Evolutionary Conserved Mechanism Timing Juvenile to Adult Transition

Derya Deveci,[1] Francisco A. Martin,[2] Pierre Leopold,[3,*] and Nuria M. Romero[1,4,*]
[1]University Côte d'Azur, CNRS, Inserm, Institute of Biology Valrose, Parc Valrose, 06108 Nice, France
[2]Cajal Institute, Av Doctor Arce 37, 28002 Madrid, Spain
[3]Institut Curie, PSL Research University, CNRS UMR3215, Inserm U934, UPMC Paris-Sorbonne, 26 Rue d'Ulm, 75005 Paris, France
[4]Lead Contact
*Correspondence: pierre.leopold@curie.fr (P.L.), nromero@univ-cotedazur.fr (N.M.R.)
https://doi.org/10.1016/j.cub.2019.01.053

SUMMARY

The onset of sexual maturation is the result of a hormonal cascade peaking with the production of steroid hormones. In animals undergoing a program of determinate growth, sexual maturation also coincides with the attainment of adult size. The exact signals that time the onset of maturation and the mechanisms coupling growth and maturation remain elusive. Here, we show that the *Drosophila* neuropeptide AstA and its receptor AstAR1 act as a brain trigger for maturation and juvenile growth. We first identified AstAR1 in an RNAi-based genetic screen as a key regulator of sexual maturation. Its specific knockdown in prothoracicotropic hormone (PTTH)-producing neurons delays the onset of maturation by impairing PTTH secretion. In addition to its role in PTTH neurons, AstAR1 is required in the brain insulin-producing cells (IPCs) to promote insulin secretion and systemic growth. AstAR1 function is mediated by the AstA neuropeptide that is expressed in two bilateral neurons contacting the PTTH neurons and the IPCs. Silencing brain AstA expression delays the onset of maturation, therefore extending the growth period. However, no pupal overgrowth is observed, indicating that, in these conditions, the growth-promoting function of AstAR1 is also impaired. These data suggest that AstA/AstAR1 acts to coordinate juvenile growth with maturation. Interesting, AstA/AstAR1 is homologous to KISS/GPR54, a ligand-receptor signal required for human puberty, suggesting that an evolutionary conserved neural circuitry controls the onset of maturation.

INTRODUCTION

In vertebrates, the onset of puberty is marked by an increased production of steroid hormones as a consequence of the activation of the hypothalamic-pituitary-gonadal (HPG) axis [1, 2]. In the hypothalamus, this transition coincides with the pulsatile secretion of gonadotropin-releasing hormone (GnRH) from GnRH neurons (GnRHn). GnRHn project their axons onto the pituitary gland, where follicle-stimulating hormone (FSH) and leuteinizing hormone (LH) intermediate hormones are produced, which in turn stimulates the production of steroids at the gonads. GnRH pulsatile secretion is the result of several excitatory and inhibitory inputs from afferent neural circuitries [3]. Among them, kisspeptin (KISS) produced by hypothalamus neurons plays a leading role [4–7]. Indeed, knockdown of the KISS receptor GPR54 in GnRHn induces hypogonadotropic hypogonadism and impaired onset of puberty [8]. Therefore, Kiss neuron activity and the regulation of GnRH secretion are crucial for steroid hormone production and puberty initiation. Despite its importance, the timed regulation of KISS and GnRH secretion relies on multifaceted mechanisms whose nature is still poorly understood [9, 10]. In many invertebrates, the control of sexual maturation also requires the production of steroid hormones. In *Drosophila*, the transition from juvenile to adult (i.e., metamorphosis) is marked by an increase in the production of ecdysone by the prothoracic gland (PG). Pioneering work in *Bombyx* and *Manduca* identified the prothoracicotropic hormone (PTTH) as a brain neuropeptide controlling ecdysone production. In *Drosophila* larvae, PTTH is produced by a pair of bilateral neurons (PTTHn), which project their axons on the PG [11–13]. *ptth* gene transcription significantly increases just before the juvenile-maturation transition (JMT), and ablation of PTTHn delays the time to metamorphosis by 4 or 5 days, highlighting the importance of this neural circuit in controlling JMT.

The onset of sexual maturation also coincides with the end of the growth period. Therefore, a coordination of growth and sexual maturation is needed to ensure proper adult size and fitness. Larval growth relies on the production and release of insulin-like peptides (Dilps) by specialized neurosecretory cells called insulin-producing cells (IPCs). As in other models, insulin-insulin growth factor (IGF) signaling (IIS) relays nutritional information to organ and tissue growth, and the release of Dilps by the IPCs relies on the presence of amino acids in the food [14–17]. Under limiting food, animals grow slowly and present delayed

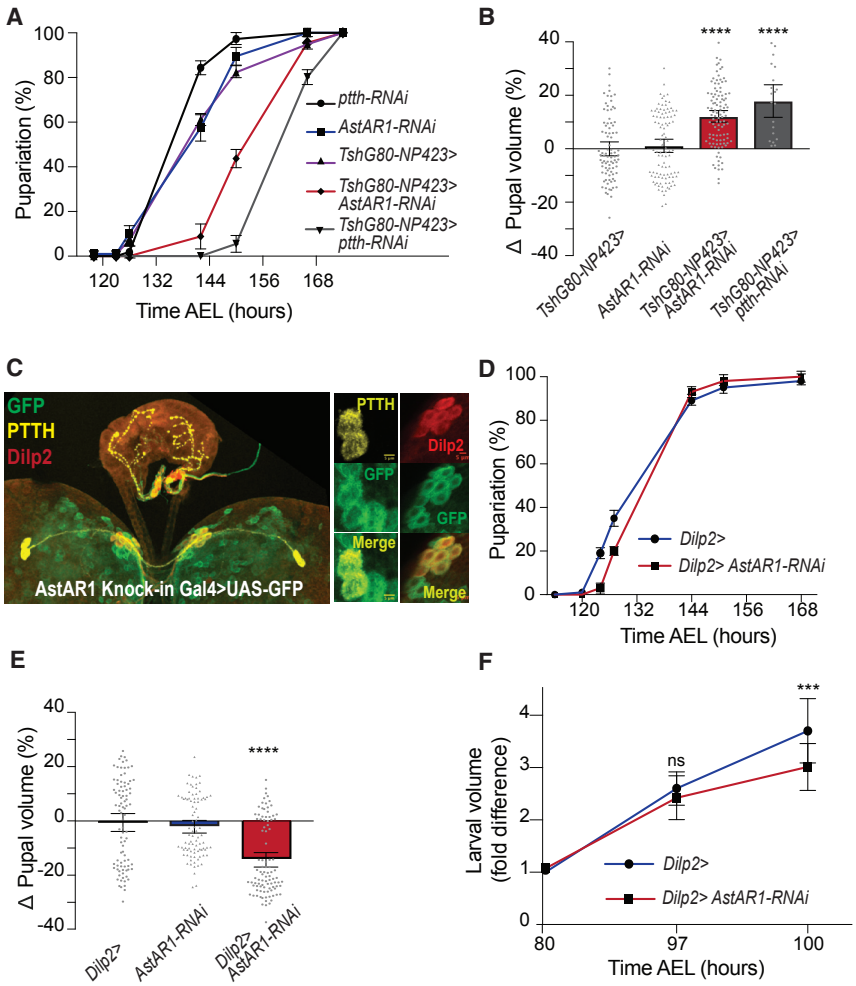

Figure 1. AstAR1 as a Positive Regulator of PTTHn and IPCs

(A and B) *AstAR1* silencing in the PTTH neurons (*TshG80-NP423>AstA-RNAi*) causes (A) a delay in metamorphosis and (B) an increase in pupal size.

(C) AstAR1 expression reporter in *Drosophila* larval brain. AstAR1 is expressed in PTTH neurons and IPCs. PTTH, IPCs, and GFP are visualized by immunostaining against PTTH (yellow), Dilp2 (red), and GFP (green).

(D and E) *AstAR1* silencing in IPCs (*Dilp2>AstA-RNAi*) (E) decreases pupal size (D) without affecting the timing of metamorphosis.

(F) This decrease of pupal size is due to a reduction in larval growth rate.

p values from pupal and larval volume are obtained via one-way ANOVA by Graphpad Prism (*p < 0.05; **p < 0.01; ***p < 0.001; ****p < 0.0001). Error bars are represented as mean ± SEM. Pupal volume data points are compared by plotting each mean value of an individual pupa in a column scatter graph obtained in Graphpad Prism. See also Figure S1.

RESULTS

AstAR1 Induces Growth and Maturation

To explore the mechanism timing the onset of JMT, we conducted an RNAi-based screen for the modulation of PTTHn activity. For this, we used the *NP423-Gal4* (*423 >*) and the *ptth-Gal4* (*ptth >*) drivers, both targeting the PTTHn. When combined with *UAS-dicer2* and *UAS-ptth-RNAi*, these driver lines induce a delay at the larva-to-pupa transition by 24 h and 12 h, respectively (Figures 1A and S1B). In addition, JMT. However, the coupling mechanism between growth and maturation is not fully understood.

Recent work has highlighted the role of a hormone called Dilp8 in another coupling between organ growth and maturation. In response to tissue damage, Dilp8 activates a neural circuit that interferes with PTTHn, ensuring extra time for tissue repair before the JMT takes place [18–20]. However, removal of Dilp8 during development does not induce premature pupariation. This suggests that in the absence of this checkpoint signal, inducer signals are still required for the timed activation of PTTHn.

In this study we performed a genetic screen aimed at identifying regulators of PTTHn. We found that allatostatin-A (AstA) and its receptor allatostatin A receptor 1 (AstAR1) control PTTH secretion, thereby determining the time of metamorphosis. Interestingly, AstA/AstAR1 also controls animal's growth rate by acting on Dilp2 secretion from the IPCs. We find that AstA/AstAR1 is developmentally regulated with a peak of activation at the onset of metamorphosis. AstAR1 is homologous to the mammalian Kisspeptin receptor, GPR54. Therefore, we propose that AstA neurons (AstAn) provide an evolutionary conserved developmental signal that controls juvenile growth and maturation, ensuring proper adult size and fitness.

the *NP423-Gal4* driver was recombined with the *TshG80* transgene to silence Gal4 expression in ventral cord neurons. We screened a collection of 1,300 RNAi constructs targeting genes encoding membrane-associated proteins, nuclear receptors, and synaptic components for their ability to delay the onset of metamorphosis when targeted to PTTHn (Figure S1A). One of our best hits identified Allatostatin-A receptor 1 (*AstAR1*), a rhodopsin-like 7 transmembrane G-coupled protein receptor, as a regulator of PTTHn function. As shown in Figures 1A, S1B, and S1C, reducing *AstAR1* expression in PTTHn by using two independent RNAi lines (*TshG80-423>AstAR1-RNAi.dcr2* or *ptth>AstAR1-RNAi.dcr2*) induces a pupariation delay similar to that observed upon *ptth* silencing (*TshG80, 423>ptth-RNAi.dcr2, TshG80, 423>ptth-RNAi2.dcr2* or *ptth>ptth-RNAi.dcr2*). As a consequence of the delayed development, larvae grow for a longer period, resulting in pupae that are approximately 10% larger than controls (Figures 1B, S1D, and S1E).

To determine *AstAR1* expression, we used an *AstAR1-Gal4* knockin line to drive GFP expression [21]. No signal was observed in larval tissues, including the gut, fat body, PG, and mitotic tissues, suggesting that *AstAR1* is mainly expressed in the brain, as previously reported by high-throughput anatomy RNA sequencing (RNA-seq) data [22]. Indeed, we observed a

signal within the brain lobes in PTTH cell bodies and PTTH axons that extend to the PG (Figure 1C). We validated *AstAR1* expression in PTTHn with two other driver lines expressing *Gal4* under the control of fragments of the *AstAR1* regulatory region [23] (Figure S1F; data not shown). Interestingly, we also detected a specific GFP signal in the IPCs, raising the possibility that AstAR1 controls the activity of these cells (Figures 1C and S1F). Indeed, silencing *AstAR1* in the IPCs using *Dilp2-Gal4* (*Dilp2 >*) and two independent RNAi lines induces an important reduction in pupal size (−14%) due to a significant reduction in larval growth rate (Figures 1E, 1F, and S1H), but it does not affect the timing of the developmental transition (Figures 1D and S1G).

Altogether, these data provide evidence that AstAR1 acts both in the IPCs and the PTTHn, exerting a dual function on the animal growth rate and the time of maturation.

AstAR1 Controls Dilp2 and PTTH Secretion

To understand the function of AstAR1 signaling in systemic growth, we analyzed Dilp2/5 expression levels in the IPCs by both immunostaining and qRT-PCR on *Dilp2*/5 transcripts. Upon *AstAR1* silencing (*Dilp2>AstAR1-RNAi*), we observed an increase in Dilp2 and Dilp5 staining in the IPCs (Figures 2A and S2A) despite normal *Dilp2* and *Dilp5* transcript levels (Figures S2B and S2C). This profile has previously been found in starved conditions to correspond to impaired Dilps secretion [16, 17]. Indeed, *Dilp2>AstAR1-RNAi* larvae show significantly reduced levels of Dilp2 in the hemolymph, as observed in starved animals (Figure 2B).

A similar approach was used to evaluate AstAR1 function in PTTHn. Because the *ptth* gene is transcriptionally controlled during development [13], we first sought to analyze *ptth* transcription but did not observe any change in *TshG80-423 > AstAR1-RNAi.dcr2* animals compared to controls (Figure S2D). Moreover, PTTH immunoreactivity remains unaffected in the PTTHn cell bodies of *TshG80-423 > AstAR1-RNAi.dcr2* larvae (Figure S2E). However, these PTTHns present extensive remodeling of their axonal terminals at the surface of PG cells with enlarged PTTH-containing boutons, reduced bouton number, and a significant decrease in the total number of axonal crosses (Figures 2D–2H). Because depolarization of the membrane is necessary for neuropeptide secretion [25], we analyzed PTTHn terminal branches after hyperpolarization of PTTHn using the inward rectifier channel Kir2.1 [26, 27]. Surprisingly, *TshG80,423 > Kir2.1* larvae show a defect in PTTH axonal terminals similar to the one observed upon *AstAR1* silencing (Figures 2E–2H), suggesting that AstAR1 may control PTTH secretion from PTTHn boutons located on the PG. To check this hypothesis, we performed ELISA tests for PTTH on larval hemolymph, a technique detecting rather important variations in circulating PTTH levels [28]. Indeed, we found lower levels of circulating PTTH in the hemolymph of *TshG80-423 > AstAR1-RNAi.dcr2* larvae compared to controls (Figure 2C).

We therefore conclude from these experiments that AstAR1 directly regulates neuropeptide secretion in both the IPCs and the PTTHn.

AstAR1 Functions Are Mediated by AstAn

The small neuropeptide Allatostatin A (AstA) is the only known ligand for AstAR1 receptor [29, 30]. Antibody stainings against AstA reveal two pairs of bilateral AstA-positive neurons (AstAns) in the larval brain [31, 32]. In order to characterize these neurons, we used an *AstA-Gal4* line from the GAL4 fly line collection (Janelia Farm), which presents an expression pattern similar but stronger than the previously described *AstA-Gal4* [33]. Driving red fluorescence protein (RFP) expression with this *AstA-Gal4* reveals two neural cell bodies in the basolateral protocerebrum, with dense arborizations in both dorsolateral and dorsomedia protocerebrum (Figure 3A; Video S1). Interestingly, PTTHn and IPCs are located in these arborization areas, suggesting that AstAn could contact both populations of neurons (Figure 3B). In order to test direct connections between AstAn and PTTHn or IPCs, we used the GFP Reconstitution Across Synaptic Partners (GRASP), which generates a GFP signal when two neuronal circuits are in molecular proximity [34]. When pairing *AstA-LexA>GFP11* with *423-Gal4>GFP1-10*, a cloud of GFP signal appears in the area of the PTTHn (Figure 3C). Additionally, we observed a robust GFP signal surrounding the IPCs when *AstA-Gal4>GFP1-10* is paired with *Dilp2-LexA>GFP11* (Figure 3D). These data suggest that AstAns make direct contact with both the PTTHn and the IPCs. By using DenMark (which marks dendritic arborizations) and anti-AstA immunostaining, we observed some AstA neuropeptide in the vicinity of both PTTHn and IPCs dendrites, suggesting that AstA could physically interact with its receptor in these neurons (Figures 3E and 3F).

To investigate the role of AstA in the control of PTTH neurons, we first sought to study the phenotype of $AstA^{sk1}$-null mutant [35]. Ast^{sk1} mutant larvae shows a delay at the onset of metamorphosis (Figure 4A), similar to the one observed after silencing *AstAR1* in the PTTHn (see Figure 1A). Despite having an extended growth period, $AstA^{sk1}$-null animals are slightly reduced in size (Figure 4B). This could be the result of an effect of AstA on the IPCs, as observed in *Dilp2>AstAR1-RNAi* animals (see Figure 1E). To confirm that AstA controls both larval growth and the time of metamorphosis as AstAR1 does, we silenced *AstA* ubiquitously using *AstA-Gal4*. *AstA>AstA-RNAi.dcr2* animals show delayed pupariation timing although no significant growth reduction (Figures 4C, 4D, and S3A for control of RNAi effect). The developmental delay in *AstA>AstA-RNAi.dcr2* animals correlates with a reduced kinetic of ecdysone production and is rescued by ectopic administration of 20-hydroxyecdysone (Figures S3B and 4C). Lastly, silencing *AstA* only in the larval brain (*syb>AstA-RNAi.dcr2*) causes a similar delay in metamorphosis (Figure 4E) and no overgrowth (Figure 4F). This indicates that AstA expressed in the brain controls growth and maturation by activating AstAR1 in the PTTHn and IPCs. To strengthen these data, we simultaneously silenced AstAR1 in PTTHn and IPCs by using *Dilp2,NP423>AstAR1-RNAi.dcr2*. Consistently, these larvae were delayed at metamorphosis without modification of their pupal size (Figures 4G and 4H), a phenotype similar to AstA loss of function. Thus, we conclude that the brain AstA neuropeptide controls growth and maturation through its receptor AstAR1 in IPCs and PTTHn, respectively.

AstA/AstAR1 Differentially Control Growth and Maturation through AstA-N1 and AstA-N2 Neurons

Our previous results suggest that AstAns form a neural circuit with the IPCs and the PTTHn to control growth and

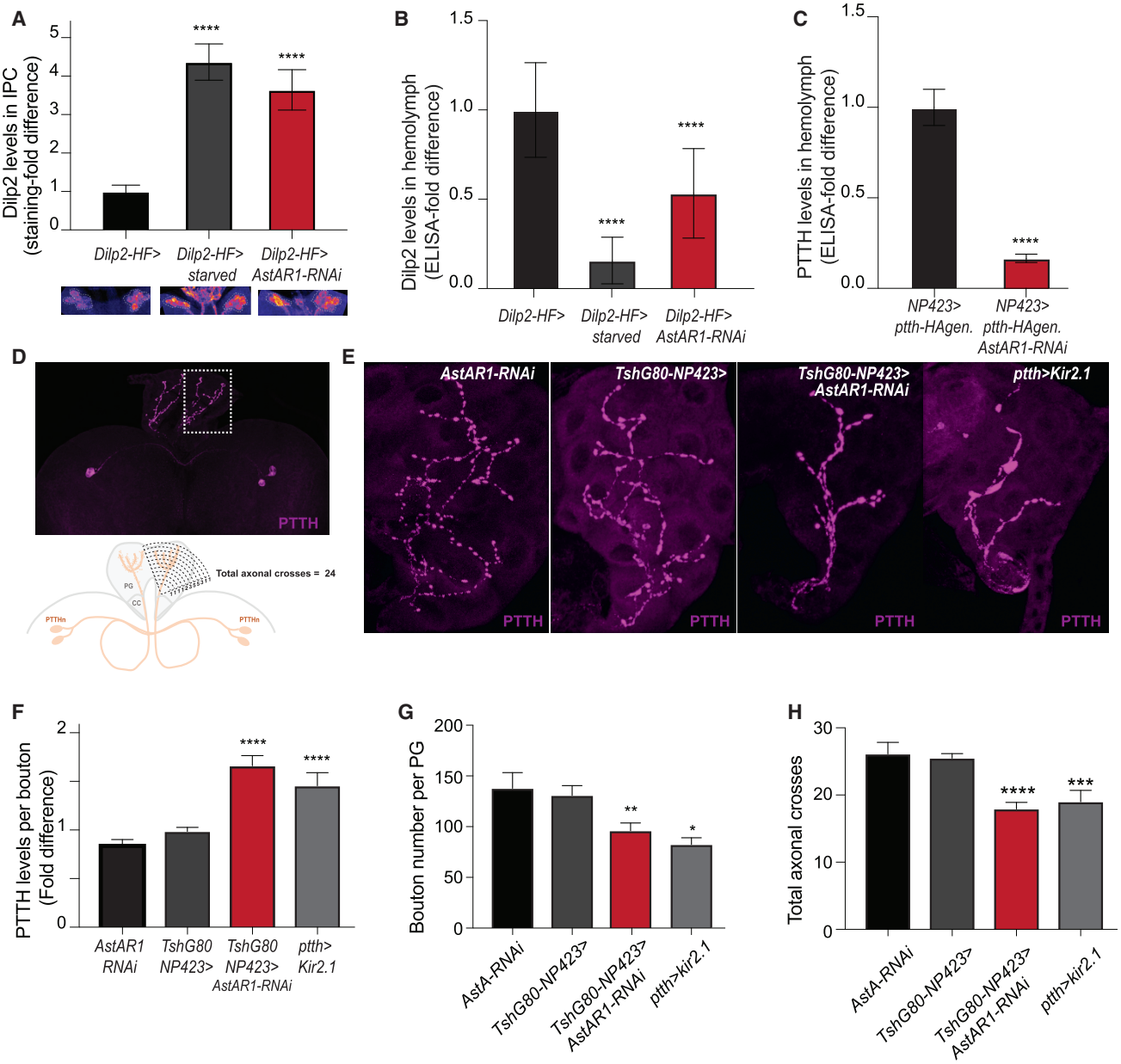

Figure 2. AstA-R1 Signaling Controls the Secretion of Dilp2 and PTTH

(A) AstAR1 silencing in the IPCs (*Dilp2>AstA-RNAi*) causes accumulation of Dilp2 in the IPC cell bodies, as observed in acutely starved larvae (positive control).

(B) Corresponding Dilp2 hemolymph levels measured by ELISA (see STAR Methods).

(C) *AstAR1* silencing in PTTHn reduced levels of circulating PTTH as measured using an hemagglutinin (HA)-tagged PTTH (see STAR Methods).

(D) PTTH axonal crosses were obtained by using an adaptation of the Sholl's method, by counting the number of each PTTH projection that crossed the centric ring in the hemicircle, starting from the PG [24].

(E) *AstAR1* silencing in PTTHn (*TshG80, NP423>AstA-RNAi*) leads to morphological changes in the PTTH boutons projecting on the prothoracic glands.

(F) These changes were accompanied with an accumulation of PTTH in the PTTHn boutons projecting on the prothoracic gland, as observed upon PTTHn hyperpolarization (*ptth>Kir2.1*).

(G and H) *AstAR1* silencing in PTTHn causes (G) a reduction in the total number of PTTH boutons per PG and (H) a reduction of the total axonal crosses by using the method described in (D). Dilp2 and PTTH levels are measured by immunohistochemistry using rat anti-Dilp2 and guinea pig anti-PTTH.

p values from Dilp2 accumulation in the IPCs and Dilp2/PTTH secretion in hemolymph are obtained via one-way ANOVA by Graphpad Prism (*$p < 0.05$; **$p < 0.01$; ***$p < 0.001$; ****$p < 0.0001$). Error bars are represented as mean ± SEM. See also Figure S2.

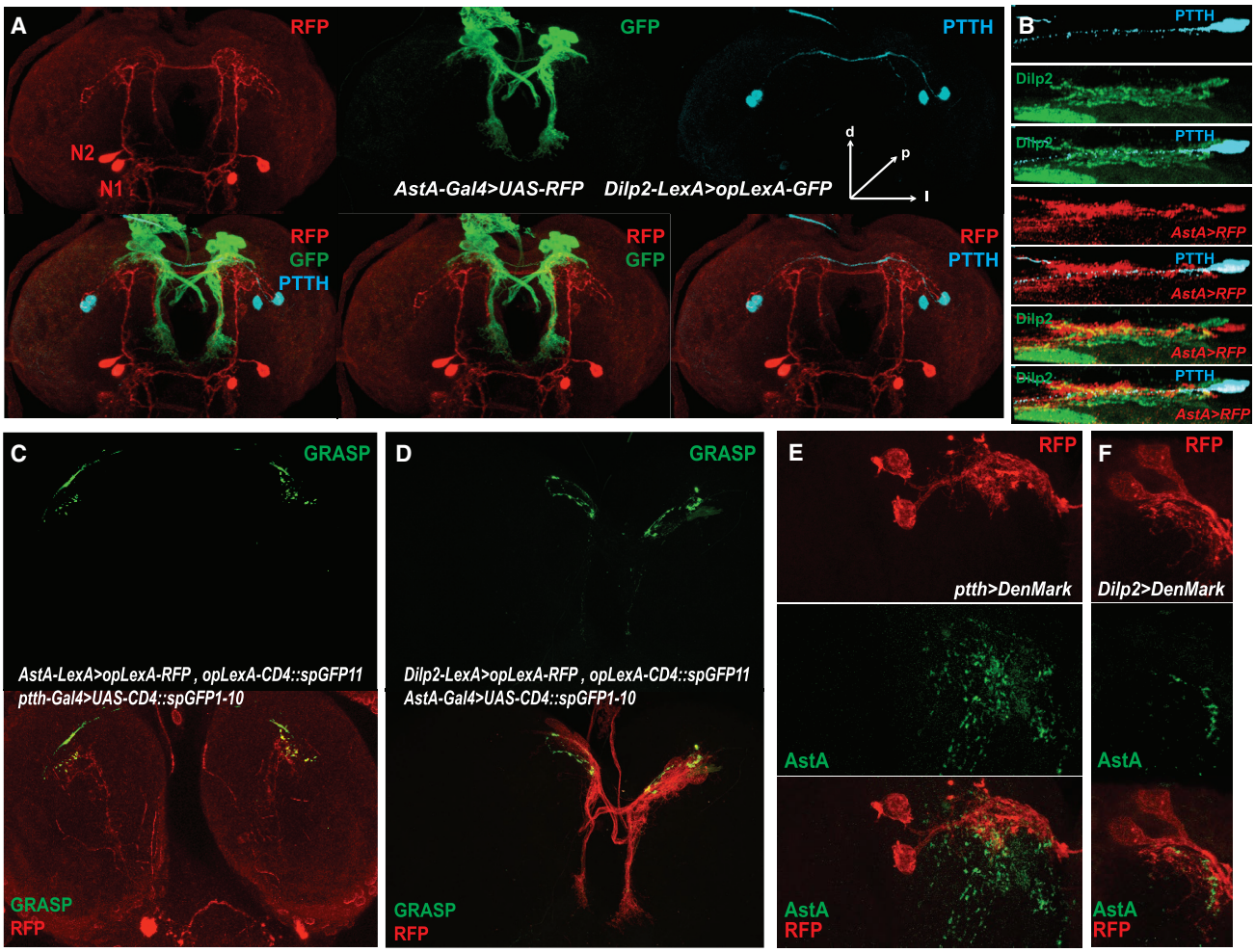

Figure 3. AstAns Make Direct Contact with PTTHn and IPCs

(A) The expression patterns of AstA and Dilp2 in larval brains are visualized using RFP and GFP, respectively (*AstA-Gal4>RFP; Dilp2-lexA>GFP*). PTTH is visualized by immunostaining (in cyan). Only one pair of bilateral neurons stain positive for GFP in the central brain (N1 and N2 neurons).

(B) XZ section of dissected larval brains labeled with RFP and GFP under the control of *AstA-Gal4* (red) and *Dilp2-LexA* (green) and stained for PTTH (cyan). Axons of the AstA-positive cells intersect with those of PTTHn and IPCs.

(C) GFP reconstitution across synaptic partners (GRASP) between AstAn and PTTHn. The GRASP signal (GFP) is in green after immunostaining against GRASP-specific GFP antibody.

(D) GRASP signal is also detected between AstAn and IPCs.

(E and F) AstA peptide localizes near the dendrites of PTTHn (E) and IPCs (F), marked by *NP423>UAS-DenMark* (red). Dendrites were marked using *NP423-Gal4>UAS-DenMark* or *Dilp2-Gal4>UAS-DenMark* (red). AstA is visualized by immunostaining (green).

See also Video S1.

sexual maturation, but it is not clear whether this is achieved commonly by both AstA neurons or whether each neuron has a distinct role. The Coin-Flp technique, which allows mosaic visualization of patterns [36], revealed the morphological diversity of AstA neurons. The main posterior AstA neuron, referred to as AstA-N1, projects anteriorly toward the PTTH projections and to some IPC projections (Figures S3C and S3D). The second AstA neuron, referred to as AstA-N2, projects toward the dorsomedium protocerebrum, where IPC cell bodies and PTTH projections are located (Figures 3A and S3C–S3E). These morphological structures suggest that AstA-N1 and AstA-N2 could signal to both PTTHn and IPCs.

In order to dissect the differential functions of AstA-N1 and AstA-N2, we use an intersection of *Gal4* and *Gal80* expression to silence individual AstA neurons. When both AstA neurons are inactivated using *Kir2.1* (*AstA>Kir2.1*), pupariation is delayed (Figure 5A) without affecting pupa size (Figure 5B), a phenotype analogous to silencing *AstA* using *AstA-Gal4* (see Figures 4C and 4D). Combining *AstA-Gal4* with *UAS-Kir2.1* and *Tsh-G80*, we could selectively silence AstA-N1 neurons, while maintaining AstA-N2 neurons active (as revealed by *GFP*; see Figure S4A). In these conditions, we observe a similar developmental delay as in *AstA>Kir2.1* animals, together with the remodeling of PTTH axon termini (Figures 4A and S4B–S4D). Once again, final pupal size is not modified, suggesting that larvae grow at a slower rate, as

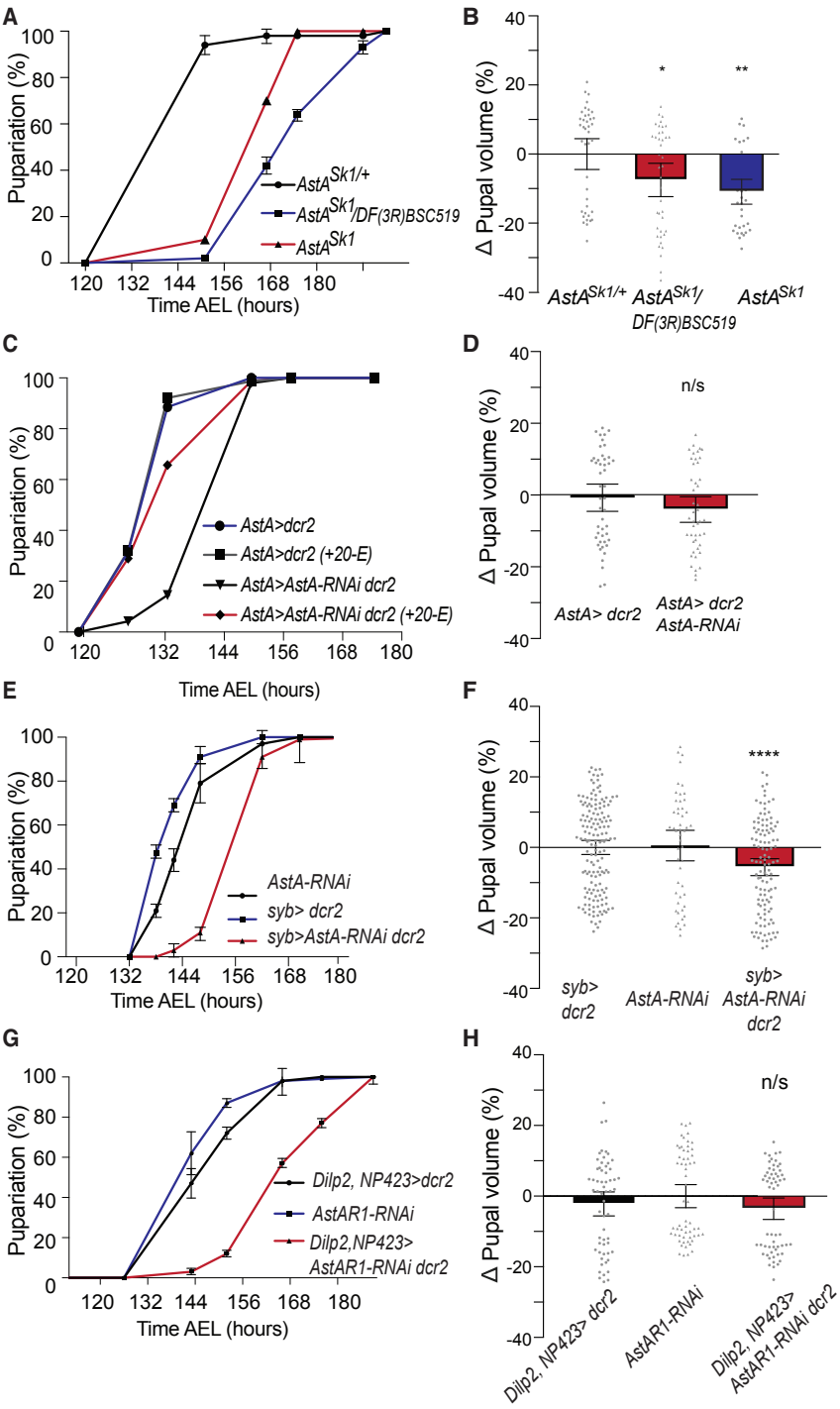

Figure 4. AstAR1-Mediated Growth and Maturation Effects Rely on AstA

(A) AstA double mutant larvae ($AstA^{Sk1}$) or $AstA^{Sk1}$/Df(3R)BCS519, a deficiency covering the AstA locus, are delayed in the onset of metamorphosis.

(B) $AstA^{Sk1}$ double mutant and $AstA^{Sk1}$/Df(3R)BCS519 animals have significantly smaller pupal volume.

(C and D) Silencing AstA (*AstA>AstA-RNAi.dcr2*) leads to (C) a delayed onset of metamorphosis (D) without affecting pupal volume.

(E and F) AstA silencing in the brain (*syb>AstA-RNAi.dcr2*) (E) delays metamorphosis and (F) reduces pupal volume compared to controls.

(G and H) Simultaneous *AstAR1* knockdown in PTTHn and IPCs (G) delays metamorphosis (H) without affecting pupal size (*Dilp2>,NP423>AstAR1-RNAi.dcr2*).

Statistical analysis of pupal volume measurements were obtained via one-way ANOVA by Graphpad Prism (*p < 0.05; **p < 0.01; ***p < 0.001; ****p < 0.0001). Error bars are represented as mean ± SEM. Pupal volume data points are compared by plotting each mean value of an individual pupa in a column scatter graph obtained in Graphpad Prism. See also Figure S3.

indicated by a slight retention of Dilp2 in IPCs (Figures 4B and S4E). The effect of AstAN1 on developmental timing and pupal size was confirmed by silencing AstA exclusively in AstAN1 (*TshG80, AstA>AstA-RNAi.dcr2*; Figures S4F and S4G). Conversely, the forced activation of AstAN1 (*TshG80, AstA>TRPA1*) slightly advanced the onset of metamorphosis (Figure 5C). In our hands, this is an indirect but highly sensitive method to monitor PTTH signaling. Indeed, in these conditions, no obvious change in circulating PTTH levels could be observed (not shown). This indicates that AstA-N1 neurons are necessary and sufficient to control the timing of pupal transition. In addition, because pupae are of normal size despite a prolonged or shorted larval period (Figures S4G and 5D), our data indicate that AstA-N1s also affect the growth rate of the larvae. Altogether, these experiments indicate that AstA-N1s control both larval growth and the timing of maturation and AstA-N2s control larval growth only.

AstA/AstAR1 Achieve Maximal Signaling Activity in PTTHn prior to Maturation

Growth takes place during larval development, and the cessation of growth occurs concomitant with the onset of maturation when PTTH levels raise [13]. Thus, we test the temporal relevance of AstA/AstAR1 signaling by evaluating *AstAR1* expression both in IPCs and PTTHn during early and late larval development. When driven with *AstAR1-Gal4*, GFP accumulates in the IPCs at constant levels during larval development, suggesting that *AstAR1* expression is not controlled by developmental cues in these cells (Figure 6A). By contrast, we detected progressively increasing GFP signal in the PTTHn during larval development (Figure 6B). Indeed, an upregulation of *AstAR1* transcript levels is observed by qRT-PCR on whole larvae toward the end of larval development (Figure S5A). We did not observe any obvious remodeling of AstAn, as shown using an *AstA>GFP* reporter (Figure S5B). However, AstA

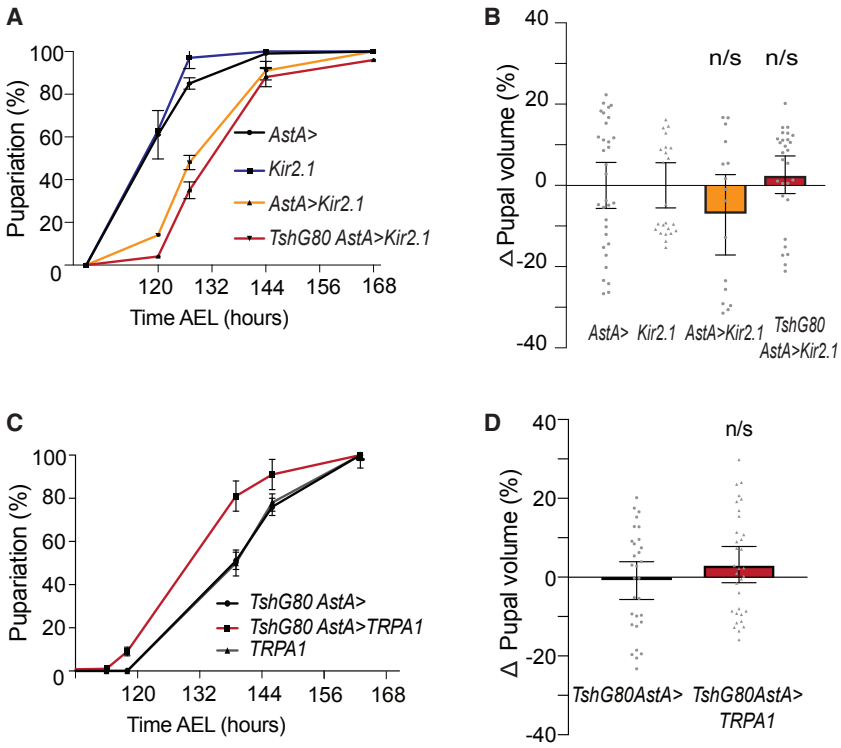

Figure 5. AstA-N1s Time the Onset of Metamorphosis and Adjust Final Pupa Size

(A) Silencing both AstAn (*AstA>Kir2.1*) or AstA-N1 alone (*TshG80, AstA>Kir2.1*) delays metamorphosis.

(B) Pupal size is decreased when both AstAns are silenced by *AstA>Kir2.1*.

(C and D) Forced activation of AstA-N1 in a temporal manner by using TRPA1 (*TshG80, AstA>TRPA1*) (C) is sufficient to advance the onset of metamorphosis (D) without changes in pupa volume.

Statistical analysis of pupal volume measurements were obtained via one-way ANOVA by Graphpad Prism (*p < 0.05; **p < 0.01; ***p < 0.001; ****p < 0.0001). Error bars are represented as mean ± SEM. Pupal volume data points are compared by plotting each mean value of an individual pupa in a column scatter graph obtained in Graphpad Prism. See also Figure S4.

immunoreactivity within AstA-N1 dramatically increases during larval development (Figure 5C). This is concomitant with the observed increase in PTTH as previously reported [28]. We could not quantify AstA peptide levels specifically in AstA-N2 as they are below detection threshold (Figure S4C). Because neuropeptides are often actively secreted by an increase in intracellular calcium [37], we used the *CaLexA* calcium reporter [38] as a marker of neurosecretory activity in these neurons. Indeed, we found increasing levels of CalexA-induced GFP in AstA-N1, suggestive of an increasing neurosecretory activity toward the end of larval development (Figure 6D).

In summary, our data indicate that AstA signals in the IPCs promote growth throughout larval development and in a temporally regulated fashion in the PTTHn to induce maturation at the end of larval period (Figure 6E).

DISCUSSION

Coordination of Growth and Maturation by AstA Signaling

During juvenile development, both the rate and the duration of growth affect final adult size. It is therefore important to clarify the mechanisms that coordinate growth rate and growth duration. Studies in *Drosophila* have revealed that PTTH plays a role in such coordination. After larvae reach a so-called critical weight, *ptth* transcripts rise, subsequently inducing a rise in ecdysone biosynthesis. In addition to this transcriptional control, we now identify AstA/AstAR1 as a signal controlling PTTH secretion. One question remains: how is the control of PTTH production coordinated with the growing status? A possible mechanism could use Dilp8/LGR3 signaling, which delays the onset of metamorphosis in response to tissue damage. Whether this signal interferes with PTTH function during normal development still needs to be clarified [18, 39]. In this study, we demonstrate that AstA signaling not only times the onset of maturation by regulating PTTH secretion but also induces larval growth by promoting Dilp secretion. Interestingly, blocking AstA signaling in the IPCs reduces larval growth rate, but this is compensated for by extending the growth period through PTTHn, allowing animals to reach normal body weight. Interestingly, another receptor for AstA, AstAR2, has been recently reported to link AstA signaling with the metabolic status in the adult IPCs [35]. Thus, AstAn, PTTHn, and IPCs likely define a homeostatic neural circuit that coordinates growth and/or metabolism and maturation timing.

AstA and KISS: A Conserved Neural Circuitry Controlling Maturation

AstA was initially described as an arthropod-specific hormone inhibiting food intake and juvenile hormone (JH) secretion [40]. However, a comprehensive evolutionary study of the AstA receptor 1 gene revealed that it shares an evolutionary ancestor gene with the mammalian GPR54 receptor gene [41]. Moreover, the *Drosophila* AstA peptide and the human KISS peptide share a conserved FGL motif, suggesting that *AstA* and *KISS* could originate from a common ancestor [41]. As previously mentioned, the KISS/GPR54 pathway promotes pulsatile secretion of GnRH, a necessary event for steroid production and sexual maturation in vertebrates [42]. In this study, we identify the AstA/AstAR1 pathway as part of the timer for PTTH secretion, ecdysone production, and the onset of sexual maturation. Our findings present unexpected functional parallels with the role of the KISS/GPR54 pathway at the onset of puberty: (1) *KISS* expression rises during pre-pubertal stages to induce maximum secretion of GnRH [43]; (2) hypothalamic levels of *GPR54* mRNA increase dramatically at pre-puberty stage [44]; and (3) an increase in KISS-GPR54 signaling occurs during puberty, due to

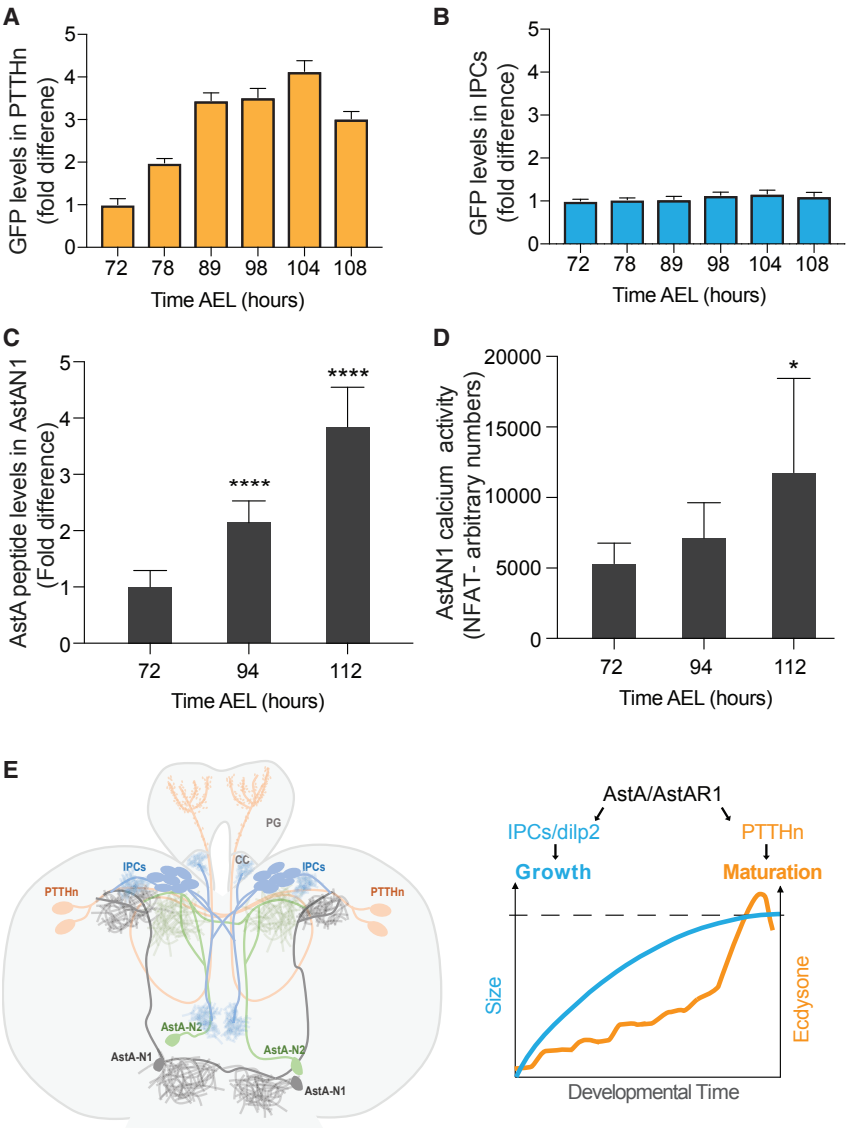

Figure 6. AstA/AstAR1 Signaling Is Developmentally Regulated

(A and B) GFP signal in *AstAR1*-knockin *Gal4>UAS-GFP* in (A) PTTHn shows gradual increase throughout larval development, whereas (B) it remains constant in IPCs. Error bars are represented as mean ± SEM.

(C) AstA peptide levels increase in the cell bodies of AstA-N1 during larval development, as detected by immunostaining against AstA. AstA peptide levels and Ca^{2+} measurements in AstA-N1 were analyzed in Microsoft Excel to obtain p values through unpaired Student's t tests (*$p < 0.05$; **$p < 0.01$; ***$p < 0.001$; ****$p < 0.0001$), and its error bars are represented as mean ± SD.

(D) Neural activity of AstAn is also increased during larval development as labeled by the CaLexA system (*AstA-Gal4>UAS-mLExA-VP16-NFAT*, *LexAop-Cd8-GFP*).

(E) Our current working model for AstA/AstAR1 signaling during larval development and schematics for AstAn/PTTHn/IPC neural network in the *Drosophila* larval brain.

See also Figure S5.

an absence of desensitization to KISS stimulus [45]. In parallel with this, we find that *Drosophila* AstA peptide levels rise at the end of development, anticipating the rise in PTTH levels and the onset of metamorphosis. Concomitantly, expression of *AstAR1* in PTTHn increases, suggesting that these neurons become more sensitive to the AstA signal just before metamorphosis. Further experiments should bring more insight into how AstA protein levels and *AstAR1* transcript rise anticipating the onset of metamorphosis. Another feature observed in mammals is the distribution of two KISS neuron subpopulations in the hypothalamus: one in the arcuate nucleus (ARC) and one in the rostral periventricular area of the 3rd ventricle (RP3V). Different roles for the ARC and RP3V KISS neurons have been allocated in either initiation or progression of puberty [46], but the regulation of these differential actions is poorly understood [5]. Similar to this, we describe here two separate AstA neurons with different functions. The sole inactivation of AstA-N1 is sufficient to induce a delay, indicating that it has clear timing function. The role of AstA-N2 in timing maturation is not yet established. Future research will be needed to better understand the differential function of AstAn and incoming regulatory signals for AstA-N1 and AstA-N2. AstA/AstAR1 signaling increases with larval volume and could respond to a size threshold. Our experiments suggest a concomitant action of AstA/AstAR1 signaling on growth and maturation. Interestingly, several studies point to the role of Kisspeptin on growth hormone (GH) secretion from the anterior pituitary gland [47–50].

Given the remarkable molecular and functional conservation between KISS and AstA signaling for the control of maturation and growth, the regulation of *Drosophila* steroid production by AstA signaling should provide further mechanical insights on this major developmental transition.

STAR★METHODS

Detailed methods are provided in the online version of this paper and include the following:

- KEY RESOURCES TABLE
- CONTACT FOR REAGENT AND RESOURCE SHARING
- EXPERIMENTAL MODEL AND SUBJECT DETAILS
- METHOD DETAILS
  - RNAi screen in PTTHn
  - Measuring developmental timing
  - AstA neuron activation by TrpA1
  - Pupal volume and growth rate measurements
  - Ecdysone titers
  - Rescue by 20-hydroxyecdysone feeding

- Immunostaining
- Quantitative RT-PCR
- Dilp2 retention in IPCs
- Circulating PTTH and Dilp2 in the hemolymph
- Quantification PTTH bouton in PG

- QUANTIFICATION AND STATISTICAL ANALYSIS

SUPPLEMENTAL INFORMATION

Supplemental Information can be found with this article online at https://doi.org/10.1016/j.cub.2019.01.053.

ACKNOWLEDGMENTS

We thank Gisele Jarretou, Thomas Phil, and Alessandra Mauri for technical assistance. We thank all members of the laboratory and the fly community for insightful discussions and comments on the manuscript. We thank the Vienna Drosophila RNAi Center, the Drosophila Genetics Resource Center, the Bloomington Stock Center, and Kyoto Stock Center for providing Drosophila lines. This work was supported by the CNRS, INSERM (Junior Researcher grant 2015/6 to N.M.R.), European Research Council (advanced grant no. 268813 to P.L.), ARC (grant no. PGA120150202355 to P.L.), and the Labex Signalife program (grant ANR-11-LABX-0028-01 to P.L.). F.A.M. is a recipient of a RyC-2014-14961 contract and supported by BFU2014-54346-JIN.

AUTHOR CONTRIBUTIONS

N.M.R. and P.L. accomplished the conceptualization. D.D., N.M.R., and F.A.M. performed the experiments and N.M.R., D.D., and P.L. designed and interpreted experiments. D.D. and N.M.R. wrote the original draft. F.A.M., P.L., D.D., and N.M.R. wrote, edited, and reviewed the manuscript.

DECLARATION OF INTERESTS

The authors declare no competing interests.

Received: July 23, 2018
Revised: November 28, 2018
Accepted: January 21, 2019
Published: February 21, 2019

REFERENCES

1. Ellison, P.T., Reiches, M.W., Shattuck-Faegre, H., Breakey, A., Konecna, M., Urlacher, S., and Wobber, V. (2012). Puberty as a life history transition. Ann. Hum. Biol. *39*, 352–360.
2. Plant, T.M. (2015). Neuroendocrine control of the onset of puberty. Front. Neuroendocrinol. *38*, 73–88.
3. Ojeda, S.R., and Skinner, M.K. (2006). Puberty in the rat. In Knobil and Neill's Physiology of Reproduction, Third Edition, J.D. Neill, ed. (Elsevier), pp. 2061–2126.
4. Navarro, V.M., and Tena-Sempere, M. (2011). Neuroendocrine control by kisspeptins: role in metabolic regulation of fertility. Nat. Rev. Endocrinol. *8*, 40–53.
5. Pinilla, L., Aguilar, E., Dieguez, C., Millar, R.P., and Tena-Sempere, M. (2012). Kisspeptins and reproduction: physiological roles and regulatory mechanisms. Physiol. Rev. *92*, 1235–1316.
6. Roa, J., Aguilar, E., Dieguez, C., Pinilla, L., and Tena-Sempere, M. (2008). New frontiers in kisspeptin/GPR54 physiology as fundamental gatekeepers of reproductive function. Front. Neuroendocrinol. *29*, 48–69.
7. Tena-Sempere, M. (2008). Timeline: the role of kisspeptins in reproductive biology. Nat. Med. *14*, 1196.
8. Herbison, A.E. (2016). Control of puberty onset and fertility by gonadotropin-releasing hormone neurons. Nat. Rev. Endocrinol. *12*, 452–466.
9. Lomniczi, A., Loche, A., Castellano, J.M., Ronnekleiv, O.K., Bosch, M., Kaidar, G., Knoll, J.G., Wright, H., Pfeifer, G.P., and Ojeda, S.R. (2013). Epigenetic control of female puberty. Nat. Neurosci. *16*, 281–289.
10. Sangiao-Alvarellos, S., Manfredi-Lozano, M., Ruiz-Pino, F., Navarro, V.M., Sánchez-Garrido, M.A., Leon, S., Dieguez, C., Cordido, F., Matagne, V., Dissen, G.A., et al. (2013). Changes in hypothalamic expression of the Lin28/let-7 system and related microRNAs during postnatal maturation and after experimental manipulations of puberty. Endocrinology *154*, 942–955.
11. Kopeć, S. (1922). Studies on the necessity of the brain for the inception of insect metamorphosis. Biol. Bull. *42*, 323–342.
12. Wigglesworth, V.B. (1934). The physiology of ecdysis in Rhodnius prolixus (Hemiptera). II. Factors controlling Moulting and "Metamorphosis". J. Cell. Sci. *77*, 191–222.
13. McBrayer, Z., Ono, H., Shimell, M., Parvy, J.P., Beckstead, R.B., Warren, J.T., Thummel, C.S., Dauphin-Villemant, C., Gilbert, L.I., and O'Connor, M.B. (2007). Prothoracicotropic hormone regulates developmental timing and body size in *Drosophila*. Dev. Cell *13*, 857–871.
14. Koyama, T., and Mirth, C.K. (2016). Growth-blocking peptides as nutrition-sensitive signals for insulin secretion and body size regulation. PLoS Biol. *14*, e1002392.
15. Delanoue, R., Meschi, E., Agrawal, N., Mauri, A., Tsatskis, Y., McNeill, H., and Léopold, P. (2016). *Drosophila* insulin release is triggered by adipose Stunted ligand to brain Methuselah receptor. Science *353*, 1553–1556.
16. Géminard, C., Arquier, N., Layalle, S., Bourouis, M., Slaidina, M., Delanoue, R., Bjordal, M., Ohanna, M., Ma, M., Colombani, J., et al. (2006). Control of metabolism and growth through insulin-like peptides in *Drosophila*. Diabetes *55*, S5–S8.
17. Slaidina, M., Delanoue, R., Gronke, S., Partridge, L., and Léopold, P. (2009). A *Drosophila* insulin-like peptide promotes growth during nonfeeding states. Dev. Cell *17*, 874–884.
18. Colombani, J., Andersen, D.S., Boulan, L., Boone, E., Romero, N., Virolle, V., Texada, M., and Léopold, P. (2015). *Drosophila* Lgr3 couples organ growth with maturation and ensures developmental stability. Curr. Biol. *25*, 2723–2729.
19. Vallejo, D.M., Juarez-Carreño, S., Bolivar, J., Morante, J., and Dominguez, M. (2015). A brain circuit that synchronizes growth and maturation revealed through Dilp8 binding to Lgr3. Science *350*, aac6767.
20. Garelli, A., Gontijo, A.M., Miguela, V., Caparros, E., and Dominguez, M. (2012). Imaginal discs secrete insulin-like peptide 8 to mediate plasticity of growth and maturation. Science *336*, 579–582.
21. Yamagata, N., Hiroi, M., Kondo, S., Abe, A., and Tanimoto, H. (2016). Suppression of dopamine neurons mediates reward. PLoS Biol. *14*, e1002586.
22. Brown, J.B., Boley, N., Eisman, R., May, G.E., Stoiber, M.H., Duff, M.O., Booth, B.W., Wen, J., Park, S., Suzuki, A.M., et al. (2014). Diversity and dynamics of the *Drosophila* transcriptome. Nature *512*, 393–399.
23. Tirian, L., and Dickson, B. (2017). The VT GAL4, LexA, and split-GAL4 driver line collections for targeted expression in the *Drosophila* nervous system. bioRxiv. https://doi.org/10.1101/198648.
24. Sholl, D.A. (1953). Dendritic organization in the neurons of the visual and motor cortices of the cat. J. Anat. *87*, 387–406.
25. van den Pol, A.N. (2012). Neuropeptide transmission in brain circuits. Neuron *76*, 98–115.
26. Baines, R.A., Uhler, J.P., Thompson, A., Sweeney, S.T., and Bate, M. (2001). Altered electrical properties in *Drosophila* neurons developing without synaptic transmission. J. Neurosci. *21*, 1523–1531.
27. Paradis, S., Sweeney, S.T., and Davis, G.W. (2001). Homeostatic control of presynaptic release is triggered by postsynaptic membrane depolarization. Neuron *30*, 737–749.
28. Yamanaka, N., Romero, N.M., Martin, F.A., Rewitz, K.F., Sun, M., O'Connor, M.B., and Léopold, P. (2013). Neuroendocrine control of *Drosophila* larval light preference. Science *341*, 1113–1116.

29. Birgül, N., Weise, C., Kreienkamp, H.J., and Richter, D. (1999). Reverse physiology in *Drosophila*: identification of a novel allatostatin-like neuropeptide and its cognate receptor structurally related to the mammalian somatostatin/galanin/opioid receptor family. EMBO J. *18*, 5892–5900.
30. Chen, J., Reiher, W., Hermann-Luibl, C., Sellami, A., Cognigni, P., Kondo, S., Helfrich-Förster, C., Veenstra, J.A., and Wegener, C. (2016). Allatostatin A signalling in *Drosophila* regulates feeding and sleep and is modulated by PDF. PLoS Genet. *12*, e1006346.
31. Yoon, J.G., and Stay, B. (1995). Immunocytochemical localization of Diploptera punctata allatostatin-like peptide in *Drosophila melanogaster*. J. Comp. Neurol. *363*, 475–488.
32. Zoephel, J., Reiher, W., Rexer, K.-H., Kahnt, J., and Wegener, C. (2012). Peptidomics of the agriculturally damaging larval stage of the cabbage root fly Delia radicum (Diptera: Anthomyiidae). PLoS ONE *7*, e41543.
33. Hergarden, A.C., Tayler, T.D., and Anderson, D.J. (2012). Allatostatin-A neurons inhibit feeding behavior in adult *Drosophila*. Proc. Natl. Acad. Sci. USA *109*, 3967–3972.
34. Gordon, M.D., and Scott, K. (2009). Motor control in a *Drosophila* taste circuit. Neuron *61*, 373–384.
35. Hentze, J.L., Carlsson, M.A., Kondo, S., Nässel, D.R., and Rewitz, K.F. (2015). The neuropeptide Allatostatin A regulates metabolism and feeding decisions in *Drosophila*. Sci. Rep. *5*, 11680.
36. Bosch, J.A., Tran, N.H., and Hariharan, I.K. (2015). CoinFLP: a system for efficient mosaic screening and for visualizing clonal boundaries in *Drosophila*. Development *142*, 597–606.
37. Südhof, T.C. (2012). Calcium control of neurotransmitter release. Cold Spring Harb. Perspect. Biol. *4*, a011353.
38. Masuyama, K., Zhang, Y., Rao, Y., and Wang, J.W. (2012). Mapping neural circuits with activity-dependent nuclear import of a transcription factor. J. Neurogenet. *26*, 89–102.
39. Garelli, A., Heredia, F., Casimiro, A.P., Macedo, A., Nunes, C., Garcez, M., Dias, A.R.M., Volonte, Y.A., Uhlmann, T., Caparros, E., et al. (2015). Dilp8 requires the neuronal relaxin receptor Lgr3 to couple growth to developmental timing. Nat. Commun. *6*, 8732.
40. Lechner, H.A.E., Lein, E.S., and Callaway, E.M. (2002). A genetic method for selective and quickly reversible silencing of Mammalian neurons. J. Neurosci. *22*, 5287–5290.
41. Felix, R.C., Trindade, M., Pires, I.R.P., Fonseca, V.G., Martins, R.S., Silveira, H., Power, D.M., and Cardoso, J.C.R. (2015). Unravelling the evolution of the Allatostatin-type A, KISS and galanin peptide-receptor gene families in bilaterians: insights from anopheles mosquitoes. PLoS ONE *10*, e0130347.
42. Navarro, V.M., Fernández-Fernández, R., Castellano, J.M., Roa, J., Mayen, A., Barreiro, M.L., Gaytan, F., Aguilar, E., Pinilla, L., Dieguez, C., and Tena-Sempere, M. (2004). Advanced vaginal opening and precocious activation of the reproductive axis by KiSS-1 peptide, the endogenous ligand of GPR54. J. Physiol. *561*, 379–386.
43. Navarro, V.M., Castellano, J.M., Fernández-Fernández, R., Barreiro, M.L., Roa, J., Sanchez-Criado, J.E., Aguilar, E., Dieguez, C., Pinilla, L., and Tena-Sempere, M. (2004). Developmental and hormonally regulated messenger ribonucleic acid expression of KiSS-1 and its putative receptor, GPR54, in rat hypothalamus and potent luteinizing hormone-releasing activity of KiSS-1 peptide. Endocrinology *145*, 4565–4574.
44. Han, S.K., Gottsch, M.L., Lee, K.J., Popa, S.M., Smith, J.T., Jakawich, S.K., Clifton, D.K., Steiner, R.A., and Herbison, A.E. (2005). Activation of gonadotropin-releasing hormone neurons by Kisspeptin as a neuroendocrine switch for the onset of puberty. J. Neurosci. *25*, 11349–11356.
45. Roa, J., Vigo, E., García-Galiano, D., Castellano, J.M., Navarro, V.M., Pineda, R., Diéguez, C., Aguilar, E., Pinilla, L., and Tena-Sempere, M. (2008). Desensitization of gonadotropin responses to kisspeptin in the female rat: analyses of LH and FSH secretion at different developmental and metabolic states. Am. J. Physiol. Endocrinol. Metab. *294*, E1088–E1096.
46. Mayer, C., Acosta-Martinez, M., Dubois, S.L., Wolfe, A., Radovick, S., Boehm, U., and Levine, J.E. (2010). Timing and completion of puberty in female mice depend on estrogen receptor alpha-signaling in kisspeptin neurons. Proc. Natl. Acad. Sci. USA *107*, 22693–22698.
47. Luque, R.M., Córdoba-Chacón, J., Gahete, M.D., Navarro, V.M., Tena-Sempere, M., Kineman, R.D., and Castaño, J.P. (2011). Kisspeptin regulates gonadotroph and somatotroph function in nonhuman primate pituitary via common and distinct signaling mechanisms. Endocrinology *152*, 957–966.
48. Kadokawa, H., Suzuki, S., and Hashizume, T. (2008). Kisspeptin-10 stimulates the secretion of growth hormone and prolactin directly from cultured bovine anterior pituitary cells. Anim. Reprod. Sci. *105*, 404–408.
49. Chang, J.P., Mar, A., Wlasichuk, M., and Wong, A.O. (2012). Kisspeptin-1 directly stimulates LH and GH secretion from goldfish pituitary cells in a Ca2+-dependent manner. Gen. Comp. Endocrinol. *179*, 38–46.
50. Gutiérrez-Pascual, E., Martínez-Fuentes, A.J., Pinilla, L., Tena-Sempere, M., Malagón, M.M., and Castaño, J.P. (2007). Direct pituitary effects of kisspeptin: activation of gonadotrophs and somatotrophs and stimulation of luteinising hormone and growth hormone secretion. J. Neuroendocrinol. *7*, 521–530.
51. Brogiolo, W., Stocker, H., Ikeya, T., Rintelen, F., Fernandez, R., and Hafen, E. (2001). An evolutionarily conserved function of the *Drosophila* insulin receptor and insulin-like peptides in growth control. Curr. Biol. *11*, 213–221.
52. Rulifson, E.J., Kim, S.K., and Nusse, R. (2002). Ablation of insulin-producing neurons in flies: growth and diabetic phenotypes. Science *296*, 1118–1120.
53. Berni, J., Pulver, S.R., Griffith, L.C., and Bate, M. (2012). Autonomous circuitry for substrate exploration in freely moving *Drosophila* larvae. Curr. Biol. *22*, 1861–1870.
54. Shimell, M., Pan, X., Martin, F.A., Ghosh, A.C., Leopold, P., O'Connor, M.B., and Romero, N.M. (2018). Prothoracicotropic hormone modulates environmental adaptive plasticity through the control of developmental timing. Development *145*, dev159699.
55. Hamada, F.N., Rosenzweig, M., Kang, K., Pulver, S.R., Ghezzi, A., Jegla, T.J., and Garrity, P.A. (2008). An internal thermal sensor controlling temperature preference in *Drosophila*. Nature *454*, 217–220.
56. Park, S., Alfa, R.W., Topper, S.M., Kim, G.E.S., Kockel, L., and Kim, S.K. (2014). A genetic strategy to measure circulating *Drosophila* insulin reveals genes regulating insulin production and secretion. PLoS Genet. *10*, e1004555.
57. Li, Q., and Gong, Z. (2015). Cold-sensing regulates *Drosophila* growth through insulin-producing cells. Nat. Commun. *6*, 10083.

STAR★METHODS

KEY RESOURCES TABLE

REAGENT or RESOURCE	SOURCE	IDENTIFIER
Antibodies		
Guinea pig monoclonal anti-PTTH	[28]	N/A
Rat monoclonal anti-dilp2	[16]	N/A
Mouse monoclonal anti-AstA	DSHB	5F10
Rabbit polyclonal anti-AstA	Jena Bioscience	ABD-062
Chicken monoclonal anti-GFP	Sigma	G6539
Alexa Fluor 488 polyclonal anti-chicken	Thermo Fisher Scientific	A11039
Alexa Fluor 488 polyclonal anti-mouse	Thermo Fisher Scientific	A11029
Alexa Fluor 546 polyclonal anti-rat	Thermo Fisher Scientific	A11081
Alexa Fluor 647 polyclonal anti-rabbit	Thermo Fisher Scientific	A31573
Mouse monoclonal anti-FLAG	Sigma-Aldrich	F1804
Chemicals, Peptides, and Recombinant Proteins		
Vectashield Mounting Medium	Vector laboratories	H-1200
Formaldehyde, 16%	Polysciences	18814-10
RNeasy lipid tissue Minikit	QIAGEN	74804
SuperScript II reverse transcriptase	Invitrogen	18064014
Power SYBR Green PCR mastermix	Applied Biosystems	4367659
F8 Maxisorp loose Nunc-Immuno modules	Thermo Scientific	469949
BuPH Carbonate-Bicarbonate buffer packs	ThermoFisher	29892
anti-HA-Peroxidase, High Affinity (3F10)	Roche	12013819001
1-Step Ultra TMB- ELISA Substrate	Thermo Scientific	34029
Critical Commercial Assays		
Spi Bio 20-HE ELISA kit	Spi Bio	A05120
20-HE	Sigma	H5142
Experimental Models: Organisms/Strains		
Drosophila NP423-Gal4	DGRC	103614
Drosophila ptth-Gal4	[13]	N/A
Drosophila Dilp2-Gal4	[51, 52]	N/A
Drosophila Tsh-Gal80	[53]	N/A
Drosophila AstA-Gal4	BDSC	39351
Drosophila ptth-HA genomic	[54]	N/A
Drosophila UAS-TRPA1	[55]	N/A
Drosophila Ilp2HF	[56]	N/A
Drosophila Dilp2-LexA	[57]	N/A
Drosophila AstAR1-Gal4	[21]	N/A
Drosophila AstA-RNAi	VDRC	14398
Drosophila AstAR1-RNAi	VDRC	39222
Drosophila AstAR1-RNAi	VDRC	48495
Drosophila ptth-RNAi	VDRC	102043
Drosophila UAS-dicer2	VDRC	60008
Drosophila UAS-dicer2	VDRC	60009
Drosophila op-LexA-GFP	BDSC	58754
Drosophila UAS-RFP	BDSC	58754
Drosophila CoinFLP-LexA::GAD	BDSC	58753
Drosophila UAS-Kir2.1	BDSC	6595

(*Continued on next page*)

Continued		
REAGENT or RESOURCE	SOURCE	IDENTIFIER
Drosophila UAS-DenMark	BDSC	33061
Drosophila UAS-CD8GFP	BDSC	32185
Drosophila DF(3R)BSC519	BDSC	25023
Drosophila nSyb-Gal4	BDSC	51635
Drosophila LexAop-rCD2-RFP;UAS-CD4-spGFP1-10, LexAop-CD4-spGFP11	BDSC	58755
Drosophila VT-204065-Gal4	VDRC	*204065*
Oligonucleotides		
ptth forward primer CGTAATGGATGCTGCTGCT	Sigma-Aldrich	N/A
ptth reverse primer GGCATCATGCTCGATCTGT	Sigma-Aldrich	N/A
Dilp2 forward primer ATCTGGACGCCCTCAATCC	Sigma-Aldrich	N/A
Dilp2 reverse primer TCCCAGGAAAGAGGGCACTT	Sigma-Aldrich	N/A
Dilp5 forward primer GCCTGTCCCAATGGATTCAA	Sigma-Aldrich	N/A
Dilp5 reverse primer AGCTATCCAAATCCGCCAAGT	Sigma-Aldrich	N/A
Software and Algorithms		
Leica Application Suite	Leica Microsystems	https://www.leica-microsystems.com
ImageJ	ImageJ- NIH	https://imagej.nih.gov/ij/download.html
Microsoft Excel	Microsoft	https://www.microsoft.com/en-us/download/details.aspx?id=10
Graphpad Prism	Graphpad Software	https://www.graphpad.com/
Other		
Leica TCS SP5	Leica microsystems	https://www.leica-microsystems.com/products/confocal-microscopes/p/leica-tcs-sp5/
Leica M205 FA	Leica microsystems	https://www.leica-microsystems.com/products/stereo-microscopes-macroscopes/p/leica-m205-fca/

CONTACT FOR REAGENT AND RESOURCE SHARING

Further information and requests for resources and reagents should be directed to and will be fulfilled by the Lead Contact, Nuria M Romero (Nuria.ROMERO@univ-cotedazur.fr).

EXPERIMENTAL MODEL AND SUBJECT DETAILS

Drosophila melanogaster strains were raised at 25°C on standard cornmeal food containing, per liter, 17 g inactivated yeast powder, 83 g corn flour, 10 g agar, 60 g white sugar, and 4.6 g Nipagin. Male and female larvae and pupas were used in all experiments. The following transgenic and mutant flies were used: *ptth-Gal4* [13], *Dilp2-Gal4* [51, 52], *Tsh-Gal80* [53], *ptth-HA genomic* [54], *Ilp2HF* [56], *Dilp2-LexA* [57], *AstAR1-Gal4* [21], *UAS-TRPA1* [55] From Vienna *Drosophila* RNAi Center we obtained the following lines: *AstA*-RNAi (#14398), *AstAR1*-RNAi (#39222), *ptth*-RNAi (#102043), *UAS-dicer2* (#60008) or (#60009). *NP423-Gal4* (#103614, *Drosophila* Genetic Resource Center, Kyoto). The following lines were obtained from Bloomington *Drosophila* Stock Center: *AstA-Gal4* (#39351), op-LexA-GFP (#58754), UAS-RFP (#58754), *CoinFLP-LexA::GAD* (#58754), *UAS-Kir2.1* (#6595), *UAS-DenMark* (#33061), *nSyb-Gal4* (#51635), opLexA-RFP, opLexA-CD4::spGFP11, UAS-CD4::spGFP1-10. For the starvation controls used for Dilp2 quantifications, larvae were starved at L3 by shifting them on agar plates containing PBS/1% sucrose and collected for tissue dissection after 15 hours (O/N). All animal experimentations were approved by the Veterinary Office of Canton de Vaud.

METHOD DETAILS

RNAi screen in PTTHn

We performed a biased genetic screen to identify to identify positive regulators of PTTHn. We used the *NP423-Gal4* line to screen a set of RNAi lines from the Vienna *Drosophila* RNAi Center (VDRC) for selected GO (Gene Ontology) terms present in the brain: membrane targeted proteins, nuclear receptors, vesicular mediated neurotransmitter components. 1300 lines were tested on their ability to delay metamorphosis. We tested 300 lines per week by crossing 16 virgins containing the *NP423-Gal4* driver with 10 males of each RNAi lines. Three replicates were collected from each cross with collections of 4 h. 270 candidates significantly affected

developmental timing. In a secondary screen, positive RNAi lines were combined with *ptth* > *ptth* > *dcr2* tester line. Only one hit presented a strong and robust developmental delay of metamorphosis, *AstAR1*.

Measuring developmental timing

All developmental timing experiments were conducted at 25°C on standard cornmeal food without added sugar. Embryos were collected after 4 hours of egglaying carried out on agar dishes containing 3% sugar and were incubated at 25°C for 21 hours after which the L1 larvae were transferred into tubes containing standard cornmeal without added sugar. Pupae number from 4 tubes per genotype were scored 3 times a day and ordered by progressive pupariation time and plotted in GraphPad or Microsoft Excel using non-linear regression curve fit.

AstA neuron activation by TrpA1

AstA neurons were activated in a temporal manner by expressing TrpA1. *TshG80-AstA* > TrpA1 animals were synchronized at the L2 to L3 transition. Larvae were then kept at 25°C and transferred to 29°C after 12 hours to activate the TrpA1-expressing neurons. Pupariation was then monitored by counting pupae over time.

Pupal volume and growth rate measurements

Larval growth rate was measured by sorting larvae at the transition of L2 into L3 and transferred to standard cornmeal food. At 80, 97 and 100 hours AEL, images of the larvae were captured under bright light by using the Leica M205 FA. Similar, to obtain pupal volume, pupae were aligned in a petridish and captured under bright light. Pupal or larval length (L) and width (W) were obtained with ImageJ by measuring the medial line between anterior-posterior, and by measuring along the axial line, respectively. Pupal or larval volume was calculated in Microsoft Excel by using the formula for prolate spheroid: $(\pi/6)W^{2*}L$. Values were normalized to one control condition to give the "Δ pupal volume." Data obtained was plotted in GraphPad to obtain bar graphs.

Ecdysone titers

Biological replicates of 4-15 larvae were homogenized twice in methanol and cleared by centrifugation to give a final combined volume of ~ 450 μl. Duplicate samples were dried and resuspended in 50 μl EIA buffer (spi bio 20-HE ELISA kit – A05120). Spi Bio Kit for 20-HE ELISA were used as per manufacturer's recommendation. The standard curve was determined using GraphPad Prism software, non-linear regression curve fit, asymmetric sigmoidal, 5PL, X is log (conc). Per animal, E titers were adjusted for the volume used in the assay.

Rescue by 20-hydroxyecdysone feeding

Forty freshly ecdysed *AstA>dcr2* or *AstA* > *AstA-RNAi.dcr2* L3 larvae, grown at 25°C were transferred to a new vial. After 20 h, larvae were washed and transferred to a vial supplemented with either 20-hydroxyecdysone (Sigma; dissolved in 95% ethanol, final concentration 0.2 mg/ml) or 95% ethanol (same volume as 20-HE). Once seeded with L3 larvae, the vials were returned to 25°C and monitored for pupariation.

Immunostaining

Dissected brains were fixed in 4% formaldehyde (Sigma) for 25 min at RT, washed in PBT (0,1% Triton X-100 in PBS (137 mM NaCl, 2.7 mM KCl, 4.3 mM Na2HPO4, 1.47 mM KH2PO4, [pH 8])) and blocked in PBT containing 10% FBS for 40 min. Brains were incubated in PBT containing the primary antibody overnight at 4°C, washed three times in PBT, incubated with the secondary antibody for 2 hours at 4°C, washed and mounted in Vectashield mounting media with DAPI (Vector laboratories). The following primary antibodies were used: α-PTTH at (1:400, guinea pig), α-dilp2 (1:400, rat), α-AstA (1:20, mouse anti Ast7 cockroach, DSHB #5F10), α-AstA (1:100, rabbit against cockroach A-AST, Jena Bioscience #ABD-062) α-GFP (1:10.000, chicken), α-GFP specifically recognizing reconstituted GRASP (1:100, mouse, Sigma). Secondary antibodies that were used: Alexa Fluor 488 α-chicken (1:400, Thermo Fisher Scientific), Alexa Fluor 488 α-mouse (1:400), Alexa Fluor 546 α-rat (1;400), Alexa Fluor 648 α-guinea pig (1:400), Alexa Fluor 648 α-rabbit (1:400). Fluorescent images were acquired with Leica TSC SP5 using the 20x or 40x objective and analyzed using ImageJ.

Quantitative RT-PCR

Larvae were washed in PBS and frozen in liquid nitrogen. Total RNA was extracted by using RNeasy lipid tissue Minikit (QIAGEN) according to the manufacturer's protocol. RNA samples were treated with DNase and then reserve transcribed to cDNA using the SuperScript II reverse transcriptase (Invitrogen). cDNA samples were then used for RT-qPCR (StepOne Plus, Applied Biosystems) upon using PowerSYBRGreen PCR mastermix (Applied Biosystems). *dilp2* and *ptth* transcript levels were obtained by ΔΔCT method using rpl49 as an internal control. In Microsoft Excel, unpaired Student's t tests were used to compare two sets of data and to obtain statistical values. Primers were designed by using the NCBI/Primer-BLAST.

Dilp2 retention in IPCs

Dilp2 levels in the IPCs were quantified upon staining larval brains at 90 hr AED with α-dilp2 (1:400, rat) as described above. Confocal Z stack images were acquired at 12 bit using 0,5 μm step size with identical laser power and scanning settings. Using ImageJ, sum-intensity of Dilp2 in the IPCs was measured to obtain the area and mean intensity value.

Circulating PTTH and Dilp2 in the hemolymph

Total circulating levels of PTTH and Dilp2 in the hemolymph were quantified by sandwich ELISA. F8 Maxisorp loose Nunc-Immuno modules (Thermo Scientific #469949) were coated and incubated overnight at 4°C with α-FLAG (2.5 μg/ml, Sigma-Aldrich F1804) (for Dilp2) or α-PTTH (1:10) in coating buffer (0,2M sodium carbonate/bicarbonate buffer, pH 9,4; BuPH Carbonate-Bicarbonate buffer packs, ThermoFisher #29892). Plates were washed with PBTw0,2% (0,2% Tween-20 in PBS) and blocked with filter sterilized PBS containing 2% BSA overnight at 4°C. The next day, plates were washed with PBTw0,2% before adding hemolymph.

Hemolymph was obtained by bleeding washed larvae on ice, and collected in 50 μL ice cold PBS. Tubes containing the hemolymph were centrifuged at 1,000 x g for one minute and supernatant was collected. The samples were then mixed with α-HA-Peroxidase, High Affinity (3F10) (Roche #12013819001) at a dilution of 1:500 in PBTw0,2% and incubated in the blocked Nunc-Immuno modules overnight at 4°C. The next day, samples were aspirated and the plates were extensively washed with PBTw0,2%. Next, 1-Step Ultra TMB- ELISA Substrate (Thermo Scientific #34029) was added into the wells and incubated for 30 min at RT. The reaction was stopped by adding 2M sulfuric acid and absorbance was measured immediately at 450nm.

Quantification PTTH bouton in PG

PTTH content per bouton was quantified upon staining wandering larvae with α-PTTH as described above. Confocal Z stack images were acquired at 12 bit using a 0,5 μm step size with identical laser power and scanning settings. Using ImageJ, sum- intensity of the PTTH boutons was measured to obtain pixel intensity and area. PTTH per bouton was obtained by pixel intensity * area. The total number of boutons were counted also in ImageJ. PTTH axonal crosses were obtained by using an adaptation of the Sholl's method, by counting the number of each PTTH projection that crossed the centric ring in the hemicircle, starting from the PG [24].

QUANTIFICATION AND STATISTICAL ANALYSIS

All experimental P values are the result of ANOVA or Student's test provided by Microsoft Excel or Graphpad Prism unless otherwise stated (*$p < 0,05$; **$p < 0,01$; ***$p < 0,001$, ****$p < 0,0001$). Statistical values (P- value) obtained from the quantification of the PTTH bouton and axonal crosses in the PG was obtained by using Two-Sample t test (Student's t test) in Microsoft Excel. P values from Dilp2 accumulation in the IPCs and Dilp2/PTTH/ecdysone in hemolymph are obtained via one-way ANOVA by Graphpad Prism. For RT-qPCR, the average relative expression was analyzed by using Two-Sample t test (Student's t test) in Microsoft Excel. Statistical analysis of pupal volume measurements were obtained via one-way ANOVA by Graphpad Prism. Error bars are represented as mean ± SEM. Pupal volume data points are compared by plotting each mean value of an individual pupea in a column scatter graph obtained in Graphpad Prism. AstA peptide levels and Ca^{2+} measurements in AstA-N1 were analyzed in Microsoft Excel to obtain P- values through unpaired Student's t tests.